ORNL/TM-2024/3401

Evaluation of Radiography for TRISO Buffer Layer Density Measurement

Grant W. Helmreich
Katherine I. Montoya
J. Wesley Jones
John D. Hunn

May 2024

Approved for public release.
Distribution is unlimited.

OAK RIDGE National Laboratory

ORNL IS MANAGED BY UT-BATTELLE LLC FOR THE US DEPARTMENT OF ENERGY

ORNL/TM-2024/3401

Nuclear Energy and Fuel Cycle Division

EVALUATION OF RADIOGRAPHY FOR TRISO BUFFER LAYER DENSITY MEASUREMENT

Grant W. Helmreich
Katherine I. Montoya
J. Wesley Jones
John D. Hunn

May 2024

Work sponsored by
US DEPARTMENT OF ENERGY
Office of Nuclear Energy—Advanced Reactor Technologies
under the
Advanced Gas Reactor Fuel Development and Qualification Program

Prepared by
OAK RIDGE NATIONAL LABORATORY
Oak Ridge, TN 37831
managed by
UT-BATTELLE LLC
for the
US DEPARTMENT OF ENERGY
under contract DE-AC05-00OR22725

CONTENTS

LIST OF FIGURES

LIST OF TABLES

ABBREVIATIONS

AGR	Advanced Gas Reactor Fuel Development and Qualification
IPyC	inner pyrolytic carbon
OPyC	outer pyrolytic carbon
ORNL	Oak Ridge National Laboratory
RCRA	Resource Conservation and Recovery Act
TRISO	tristructural isotropic
XCT	x-ray computed tomography

ABSTRACT

Tristructural isotropic (TRISO) fuel particles consist of a central uranium-bearing kernel and a series of coating layers designed to retain fission products and to ensure fuel performance. Several parameters such as thickness and density must be measured for these coating layers to show that they conform with fuel specifications. Current methods for measuring the density of pyrolytic carbon and silicon carbide layers (liquid gradient density column) and the buffer layer (mercury porosimetry) generate Resource Conservation and Recovery Act (RCRA) radiological-mixed waste. In addition, measurement of buffer and inner pyrolytic carbon layer densities require hot sampling or interrupted coating runs and the mercury porosimetry method used for buffer density measurement only measures the mean buffer density, not the interparticle distribution. A new approach has been evaluated to measure the density of coating layers in TRISO particles based on the dependence of x-ray attenuation in radiographs on material density. This method does not generate RCRA mixed waste, measures density on a particle-by-particle basis, and in principle is capable of measuring the density of all coating layers in a single process. Initial results using thinned TRISO particle sections to evaluate radiography measurement of density as a quality control characterization method are reported herein. In this work, the primary focus is on measurement of the density of the buffer layer; however, with appropriate calibration the method should be applicable to other coating layers. Improvements to the initial method and a full demonstration of the method on the remaining coating layers may be pursued as a future effort.

1. CONSIDERATIONS FOR BUFFER DENSITY MEASUREMENT

The density of the buffer layer is an important attribute in tristructural isotropic (TRISO) fuels because it is the plenum for fission gas retention within the particle, provides material that shields the inner pyrolytic carbon layer from fission product recoil, and accommodates kernel swelling without transmitting excess stress to the outer structural layers responsible for retaining fission products within the particle. Ideally, buffer layer density would be measured in the final, fully coated particle and it would be measured on an individual particle level to allow for the determination of the statistical distribution of buffer density within a batch, rather than just the mean value. However, the open porosity of the buffer layer prevents measurement of the layer envelope density of individual layer fragments using a liquid gradient density column as is done with other coating layers. Thus, the current method generally used for measurement of buffer density is determination of the mean envelope volume and mass of buffer-coated particles acquired from interrupted coating runs or hot sampling before inner pyrolytic carbon (IPyC) deposition followed by subtraction of the mean envelope volume and mass of the associated kernel lot for calculation of mean buffer envelope density [1]. This method is the industry standard; however, it generates a mixed RCRA waste stream containing high-assay low-enriched uranium and mercury, it cannot measure the buffer density on the fully coated particles, and it does not allow for measurement of the buffer density on individual particles as would be necessary to determine statistical intervals for the mean density and critical limits.

In previous unpublished work, the authors have attempted to improve on the existing method for buffer density measurement using optical microscopy of particle cross-sections with both as-fabricated particles and with impregnation of pores within the buffer using fluorescent dye. However, the accuracy of this approach was unreliable due to the high sensitivity of the final density to the exact thresholding parameters used to identify pores, and, in general, the observed pore volume was insufficient to fully account for the low density of the buffer layer. This observation was later supported by focused ion beam scanning electron microscopy work performed on buffer samples from TRISO particles, which showed that even at much higher resolution a substantial fraction of the low buffer density could not be accounted for based on observed porosity [2].

Considering this prior experience, this work pursued a new method based on the dependence of x-ray attenuation on the material density. Similar approaches have been applied for other materials in the past [3]. If successful, this approach would allow for relatively rapid measurement of buffer density on individual, fully coated TRISO particles, and could be extended to measure the density of all coating layers with a single method.

2. THEORY OF RADIOGRAPHY DENSITY MEASUREMENT

The attenuation of x-rays in a generic material is described by the Beer-Lambert law given in Eq. (1), where I is the transmitted x-ray signal, I_0 is the incident x-ray signal, μ is the material attenuation coefficient, and t is the thickness of the material [4].

$$I = I_0 \times e^{-\mu t} \tag{1}$$

The material attenuation coefficient μ is dependent on the energy of the incident x-rays as well as the density (ρ) and the atomic composition of the material. Since the density of material samples may vary, x-ray mass attenuation coefficients are defined as μ/ρ and are commonly tabulated as a function of x-ray energy [5]. Although, in theory, this allows for a determination of the density of a material of known composition and thickness based on x-ray attenuation, calculating this directly would rely on a precise knowledge of the energy spectrum of the incident x-rays, which is non-trivial. Therefore, two general methods have been developed to determine the density of samples using polychromatic x-ray sources.

The first method relies on calibration of a system operating at a given set of parameters using standards of known thickness and density, and with the same chemical makeup as the samples being measured [6]. A calibration curve can then be produced by rearranging Eq. (1) into Eq. (2), where ρ_s and t_s are the density and thickness of the standards, respectively. With this formulation, plotting the negative natural logarithm of the transmitted x-ray intensity divided by the known standard density against the known standard thickness results in a line with a slope equal to the mass attenuation coefficient μ/ρ for that material under those imaging parameters.

$$-ln\left(I/I_0\right)\Big/_{\rho_s} = \mu/\rho \times t_s \tag{2}$$

The other approach, which can be used if standards of known density and thickness of the material in question are not readily available, requires imaging of known standards of a material at various x-ray source accelerating voltages to determine some constants related to the x-ray spectrums generated, which can then be applied to the material of interest when imaged at the same set of x-ray source accelerating voltages to determine the material density [7]. Because of the ready availability of graphite samples of known density and thickness for calibration, the simpler approach based on calibration with a reference material at a single source energy was followed in this work.

3. PREPARATION OF TRISO PARTICLE SPHERICAL SEGMENTS

Resolving x-ray attenuation due to interaction with multiple layers of a TRISO particle would be highly challenging due to the complexity of quantitatively tracking x-ray interaction with multiple materials resulting in differential beam hardening across the sample. Two methods were considered and rejected using full TRISO particles. The first was full x-ray computed tomography (XCT) of individual particles with the relative intensity in the resulting 3D image referenced to the intensity of standards of known density. This method was rejected as being too slow to be practically implemented at scale, as XCT of individual particles requires hours of scan time to produce high quality images. The second rejected method

was radiography of full individual particles. Each pixel in the acquired radiographs would have attenuation resulting from the combined path lengths of each layer along the projected x-ray path. In theory, the x-ray attenuation through each layer could be calculated using energy-dependent attenuation coefficients following an iterative approach that starts from the pixels representing outer pyrolytic carbon (OPyC) attenuation only to calculate the OPyC density, then pixels representing OPyC and SiC attenuation to calculate the SiC density, and proceeding in the same manner until the densities of each layer are calculated. This method was rejected due to concerns regarding the necessary assumptions of sphericity and layer uniformity required to determine layer path lengths and whether sufficient low-energy x-rays to assess the inner layer densities would be present after beam-hardening by the SiC layer; however, it may be pursued at a later time if the selected method based on spherical segments proves unworkable.

Therefore, a method was developed to prepare 100–200 µm thick spherical segments through the midplane of TRISO particles (i.e., parallel-faced sections taken from the center of the sphere). This thickness was sufficient to provide a substantial areal region within the buffer for which there was no occlusion by either the kernel or the other coating layers in the density radiographs (i.e., images of the transmitted intensity of x-rays normally incident to the parallel faces of the segment). As shown in Figure 1, for a spherical segment from a TRISO particle with a 425 µm diameter kernel and standard coating layer thicknesses, approximately 80-95% of the cross-sectional area of the buffer will be unoccluded by the kernel or the other coating layers. This fraction was deemed to be sufficient for accurate measurement of the average buffer density given that thinner samples reduced the already low x-ray attenuation of the buffer layer even further and were highly fragile. In Figure 1, the OPyC layer is deemed to be occluded by the surrounding air where the OPyC layer does not extend through the full thickness of the spherical segment.

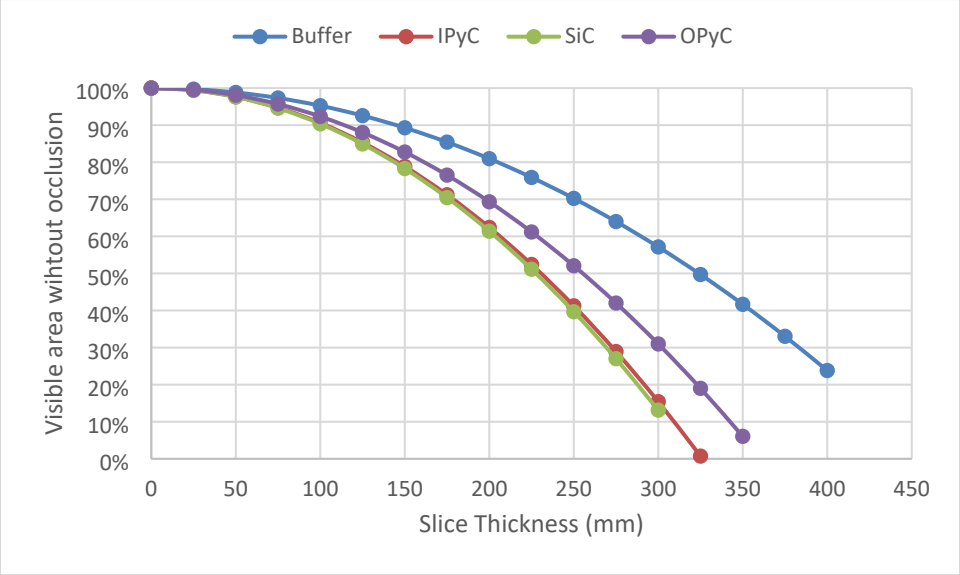

Figure 1. Visible area without occlusion from other layers for each layer within a central spherical segment of a TRISO particle of nominal dimensions.

Particles were mounted to a micrometer-controlled PELCO 15000 Lapping Fixture (Ted Pella) in a monolayer with Crystalbond Clear 509. Then, the micrometer on the fixture was set to the desired polish-down distance that would remove material equal to half the particle diameter minus half the desired spherical segment thickness of 100–200 µm. Using 600-grit SiC paper and using isopropanol as a polishing lubricant, the samples were then ground down until the sample was flush with the fixture. The mount was soaked in acetone to remove the Crystalbond Clear 509 allowing the particles to be released and mounted on flat side down. Then, the other side was ground down to the same polish down distance to result in

spherical segments centered near midplane. After grinding was complete, samples were cleaned in acetone to remove any residual polishing debris and Crystalbond, and then sandwiched between two 0.0025 in thick Kapton stickers.

4. CALIBRATION OF X-RAY ATTENUATION WITH GRAFOIL

Grafoil of two different thicknesses (0.005 in and 0.010 in) with a purity of ≥99.8% metals basis was purchased from VWR and used for fabrication of calibration reference standards. Standards ranging from 0.005 in thick to 0.040 in thick were produced by cutting small squares from the foil sheets of differing thicknesses, stacking the squares atop one another, and sandwiching the stacks between pairs of 0.0025 in Kapton stickers identical to the ones used for holding TRISO particle spherical segments. The use of identical encapsulation for the calibration standards and the samples was necessary to ensure that both sets were exposed to the same filtered x-ray spectrum. One additional calibration standard was made with no Grafoil, consisting of only two Kapton stickers adhered to each other. This blank standard was used to reference all calibration images.

Since the density of the calibration material has a direct impact on the measured density of the samples, an independent measurement of the Grafoil density was made by cutting rectangles from each sheet as to weigh ~3–5 g in total. The volume of each rectangle was calculated based on the measured side lengths (using a ruler accurate to 1/8 in) and the known Grafoil thickness (which was confirmed with calipers accurate to 0.005 mm). The mass of each rectangle was measured using a balance accurate to ±2E-4 g. Using this method, the 0.005 in thick Grafoil sheet was found to have a density of 1.26±0.07 g/cm^3, and the 0.010 in thick Grafoil sheet was found to have a density of 1.15±0.06 g/cm^3. Both of these values are slightly higher than the reported typical density of Grafoil (1.12 g/cm^3), however, the manufacturing process used for Grafoil is mechanical rolling, in which the thickness of the final material is tightly controlled, but the density may vary. The total density of each calibration standard was calculated using the composite of the two Grafoil sheet densities and the relative thickness of each used.

A challenge with source stability over time was identified during calibration. It was found that the intensity of the source shifted measurably over the time required to take a series of long-exposure radiographs for density measurement. To assess whether the source would eventually stabilize, a series of blank reference images were taken every 2 min over a 14 h period and the mean reference image intensity was plotted over time, as shown in Figure 2. Even at the end of that period, the source still appeared to be warming up based on the steadily increasing image intensity. It was found that this effect could be minimized by running the source for tens of minutes at higher power than would be used for buffer density measurement; however, it was still necessary to take reference images before and after each sample image was taken to minimize error due to shifts in the source intensity.

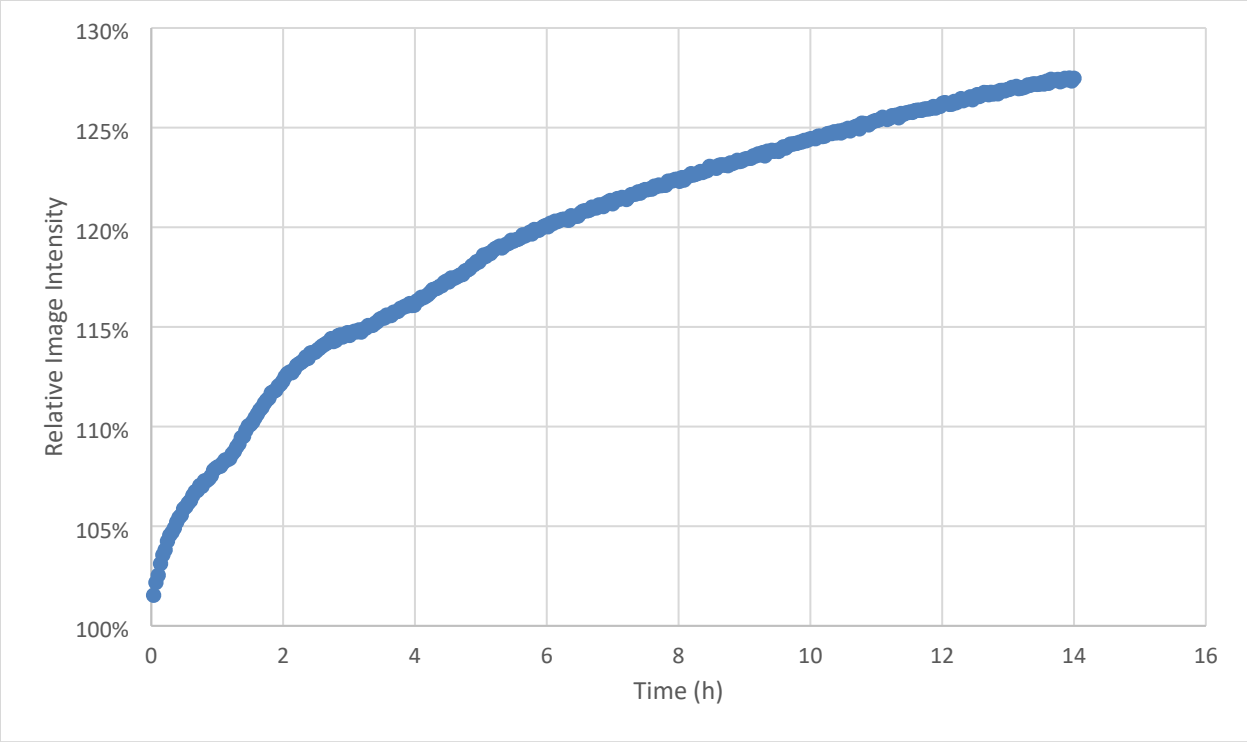

Figure 2. Mean reference image intensity as a function of time.

Based on the experience with source intensity shifting over time, calibration was performed by alternating between reference images of the empty pair of Kapton stickers and calibration images of the Grafoil encapsulated in Kapton stickers. A source-to-sample distance of 100 mm, a sample-to-detector distance of 20 mm, and the 20× objective were used, resulting in a voxel size of 0.561 µm. A source accelerating voltage of 40 kV was selected to maximize attenuation by the low-Z carbon materials being used with the maximum power of 3 W and an imaging time of 60 s. Each calibration image was referenced to the average of the two reference images preceding and following the calibration image to minimize the impact of source intensity variation. The negative natural logarithm of the calibration image intensity over the reference image intensity divided by the measured density of the Grafoil was plotted as a function of the Grafoil thickness, as shown in Figure 3. Based on Eq. (2), the linear fit through these points will have a slope equal to μ/ρ, which was found to be 1.645 cm^2/g. The overall quality of the fit is quite good, with an R^2 value of 0.9978; however, the point furthest from the fitted line is at the lowest thickness of Grafoil (125 µm), which is unfortunately the point most relevant to measurement of the ~100–200 µm thick spherical sections. Uncertainty bounds for each calibration point in Figure 3 were generated using the uncertainty in the Grafoil thickness based on caliper measurements and the propagated uncertainty in the calculated density of the two different thickness Grafoil sheets.

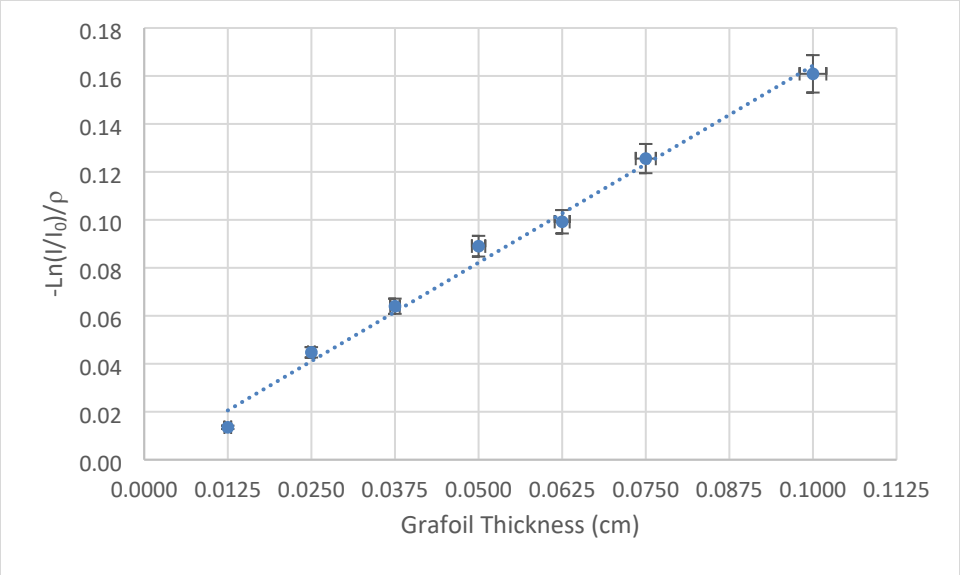

Figure 3. Calibration curve for x-ray attenuation created using Grafoil.

5. LAYER DENSITY RESULTS FOR TEST SAMPLES

Spherical sections of particles from ZrX05-31T and ZrX05-33T were produced using the method described in Section 3 to test the developed method for buffer density measurement by radiography. These are surrogate batches of particles produced for the Advanced Gas Reactor Fuel Development and Qualification (AGR) program at ORNL, and the density of the carbon-based layers measured when the material was fabricated are given in Table 1.

Table 1. Carbonaceous layer densities for ZrX05 surrogate TRISO batches used

Material	Buffer Envelope Density* (g/cm^3)	IPyC Sink/Float Density* (g/cm^3)	OPyC Sink/Float Density (g/cm^3)
ZrX05-31T	1.034	1.9089	1.9094
ZrX05-33T	1.034	1.9089	1.8752

*Note: Buffer envelope density and IPyC sink/float density were measured on interrupted coating runs using the same deposition parameters as the material batches of interest, while OPyC sink/float density was measured on the actual batches.

Front and side views of the spherical sections imaged from each material batch are given in Figure 4–Figure 9. Note that in some particles the kernel dropped out during grinding, which does not affect the results. As shown in Figure 4, because of the lower thickness of the spherical slices from ZrX05-31T and flex in the encapsulating Kapton tape it was difficult to position the sample such that the particles could be individually measured from the side. Thus, the Kapton tape was cut, and the particles were aligned as close as possible to the stage mount to minimize flexing. As a result of this, only a single thickness measurement was taken for all five particles from ZrX05-31T. The side views of both particle sets show that some tilting of the particles occurred, which will affect the actual path length through the buffer layer. No correction was made for tilting in this initial work. In addition, the side views of spherical sections from ZrX05-33T show that the sample preparation method did not remove material evenly from each side, which reduced the unoccluded area from the theoretical estimate from Figure 1. The side view images for each particle were used to determine the area in the front view images for which x-rays passed through the buffer layer only, and only that area was used for determination of mean x-ray attenuation.

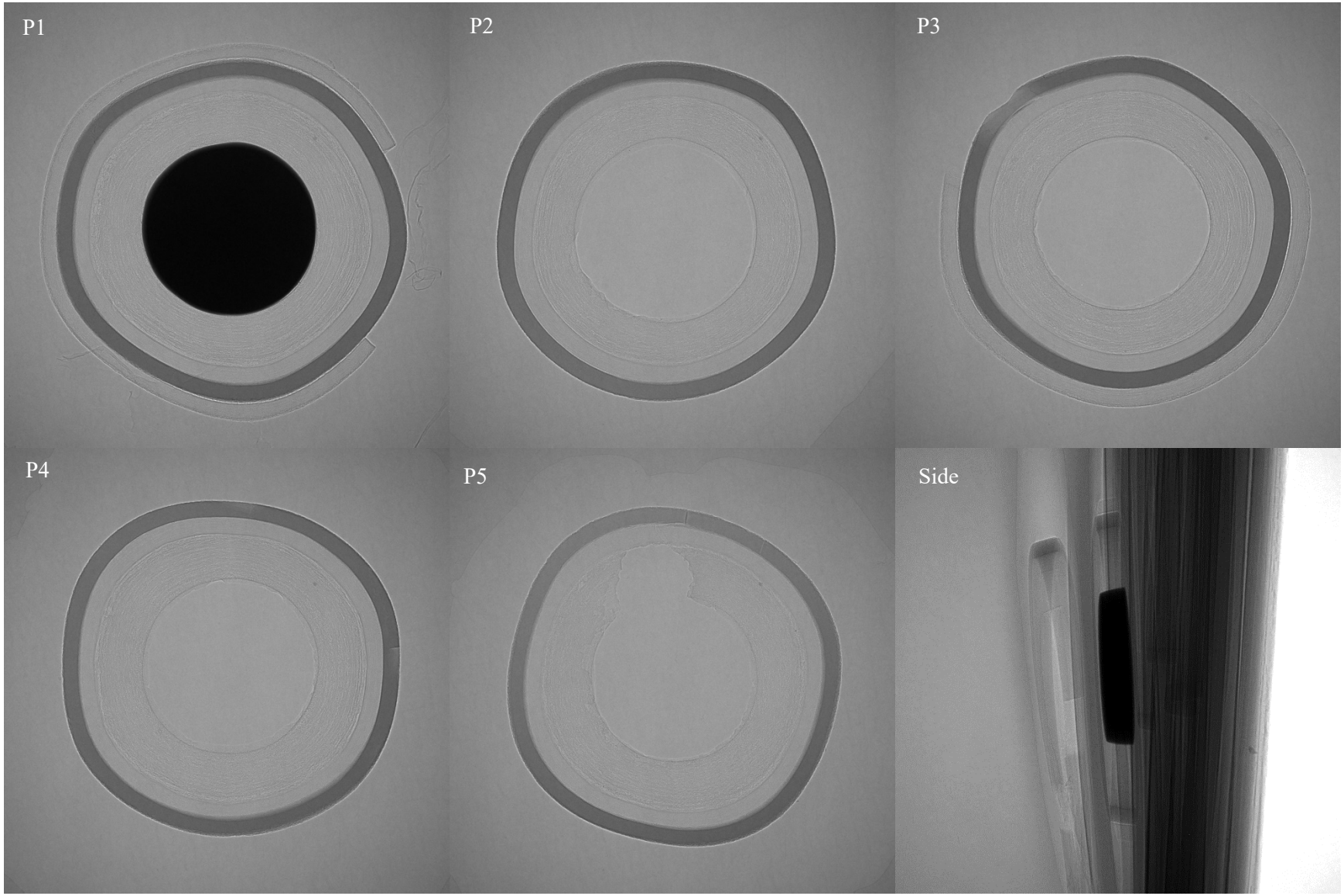

Figure 4. Radiographs of particles from ZrX05-31T.

Figure 5. Front and side views of ZrX05-33T P1.

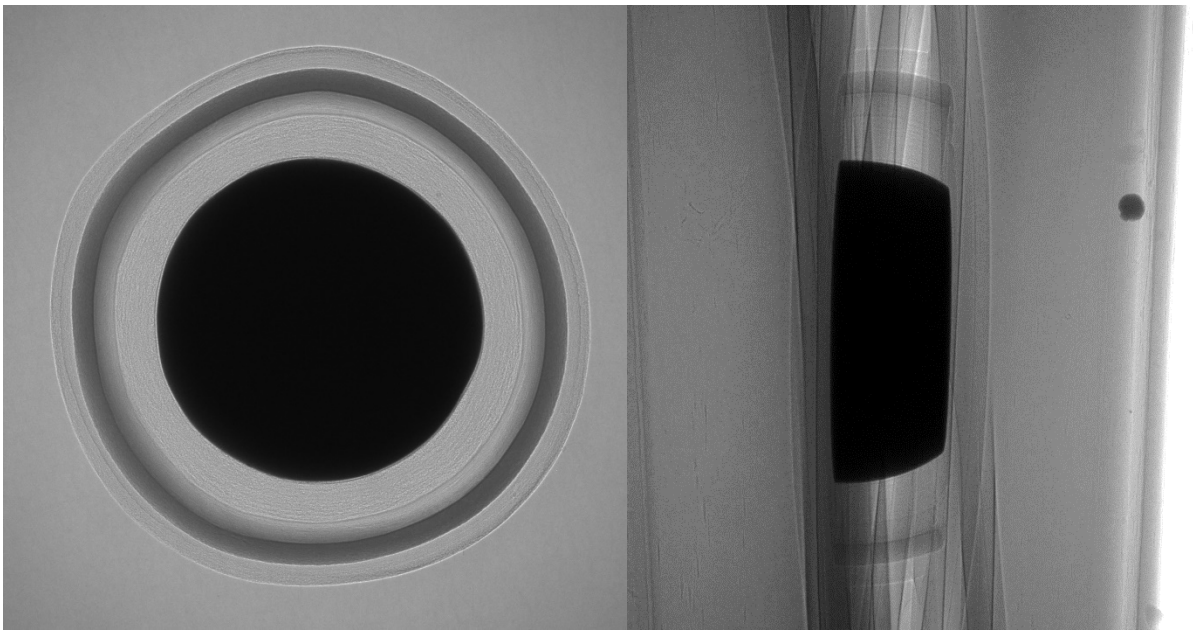

Figure 6. Front and side views of ZrX05-33T P2.

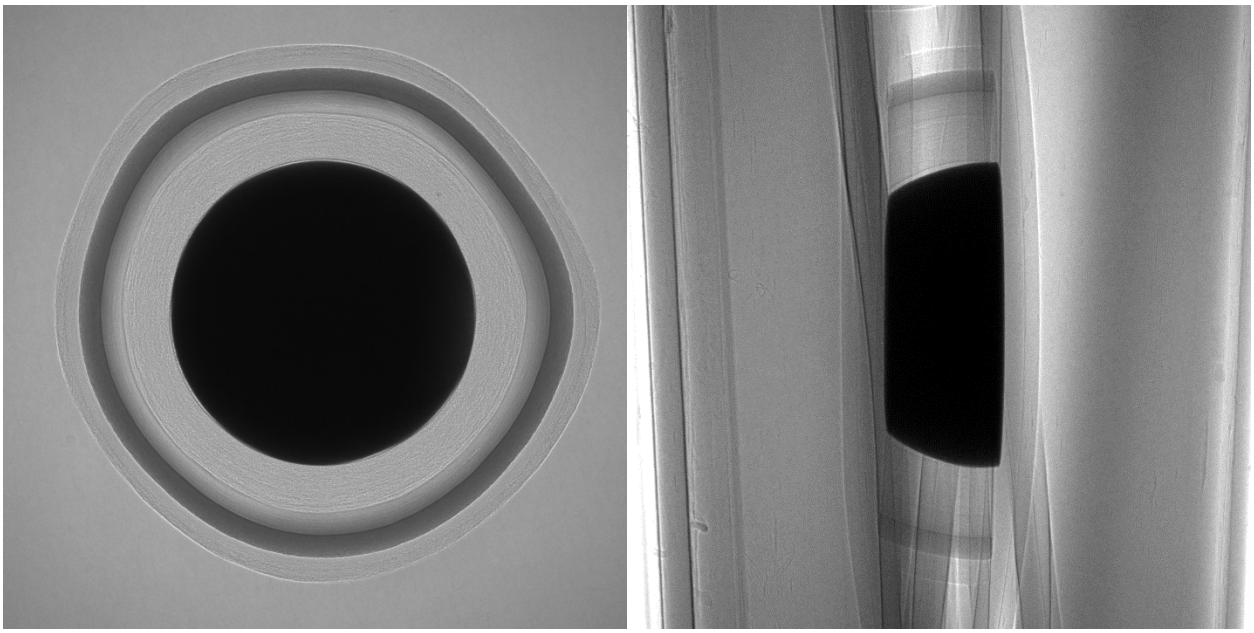

Figure 7. Front and side views of ZrX05-33T P3.

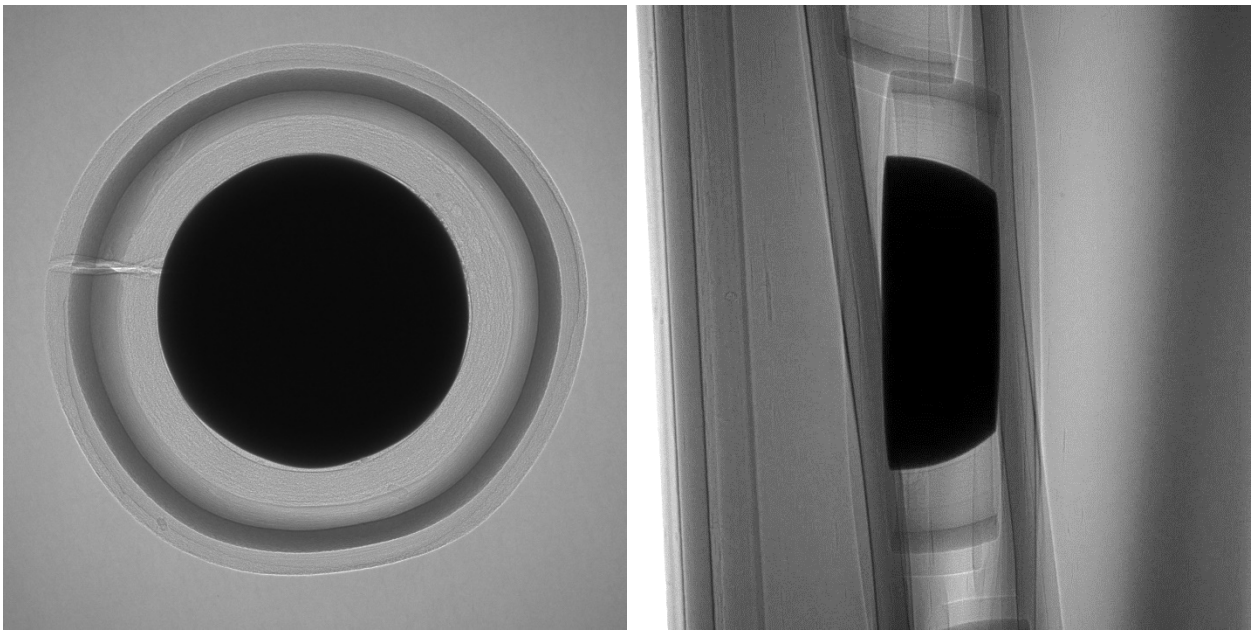

Figure 8. Front and side views of ZrX05-33T P4.

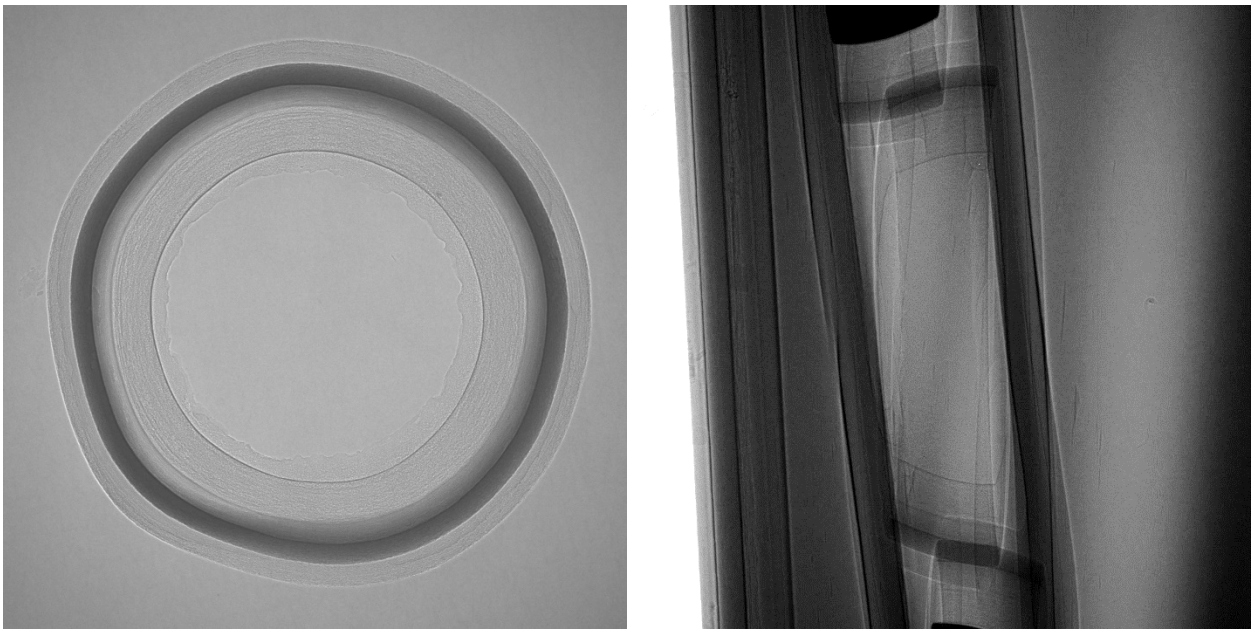

Figure 9. Front and side views of ZrX05-33T P5.

The thickness of each spherical section, the mean transmission of x-rays within the selected buffer-only area, and the resulting calculated density of the buffer layer for each particle analyzed are given in Table 2. There is a wide range in the calculated buffer densities ranging from 0.741–2.322 g/cm^3 with an average of 1.782 g/cm^3.

Table 2. Measured attenuation and calculated density for the buffer layer of radiographed spherical sections

Material	Particle	Thickness (μm)	Transmission	Density (g/cm^3)
ZrX05-33T	P1	178	0.9595	1.411
	P2	179	0.9347	2.295
	P3	176	0.9411	2.093
	P4	179	0.9357	2.259
	P5	177	0.9483	1.825
ZrX05-31T	P1	80	0.9699	2.322
	P2	80	0.9842	1.210
	P3	80	0.9737	2.025
	P4	80	0.9903	0.741
	P5	80	0.9834	1.272

The range of calculated buffer densities between particles and the bias of the average to significantly higher than the nominal buffer layer density indicate several potential issues with the initial test of the method. The primary presumed source of uncertainty is that some of the Crystalbond used to affix the particles to the lapping fixture for grinding may have infiltrated pores within the buffer and not been removed by the final acetone cleaning. There is some evidence of residual Crystalbond in the front view image of ZrX05-33T P5, shown in Figure 9, in which some material is visible inside the buffer where the kernel has dropped out. Presumably residual Crystalbond which has penetrated the buffer porosity would be even more resistant to removal. Variation in the degree of residual Crystalbond infiltrating the buffer layer of each particle would explain both the variation in calculated density and the bias towards greater

x-ray attenuation than would be expected given the sample thicknesses and the nominal density of the buffer layer.

Other less-impactful potential sources of measurement uncertainty are errors in sample thickness due to sample tilt, which would result in <2% relative error for a tilt of less than 10 degrees, and uncertainty in identification of the sample edge. These errors in sample thickness measurement would have a direct impact on the calculated density using Equation 2. In addition, the calibration curve shown in Figure 3 fits closely to most of the calibration points, but goes above the calibration point for the lowest thickness reference material, which is the most representative of the thickness of the spherical sections measured. While the calibration curve should be linear, it is possible that some non-linearity is introduced by the encapsulating Kapton tape or uncertainties in the densities of the two thicknesses of Grafoil used. If the calibration were adjusted to better fit this point the fitted slope would be higher, reducing the calculated buffer densities. However, this type of systemic bias would not account for the stochastic variation observed between samples.

While neither dataset resulted in densities close to the nominal density of the buffer layer of 1.034 g/cm^3 (Table 1), the spread in the measured values for the thinner sample (ZrX05-31T) was substantially greater than for the thicker sample (ZrX05-33T). This is likely a result of thinner samples being more susceptible to minor variations in x-ray transmission resulting in a large variation in calculated density. As shown in Figure 10, the calculated density of thinner samples is much more sensitive to changes in measured x-ray transmission. For a 100 µm thick sample, every 1% change in x-ray transmission results in a 0.64 g/cm^3 change in calculated density, while for a 250 µm thick sample, every 1% change in x-ray transmission results in a 0.26 g/cm^3 change in calculated density. Some of the variation in the measured densities may have also come from uncertainties in the measured x-ray transmission, which could have been impacted by source stability between imaging the sample and the blank Kapton reference, as discussed in Section 4, or by the detector resolution to x-ray intensity. The sensitivity of calculated density to variations in x-ray transmission may be reduced either by using thicker samples or by removing the encapsulating Kapton tape, which absorbs some low energy x-rays and thereby reduces the overall attenuation in the actual sample.

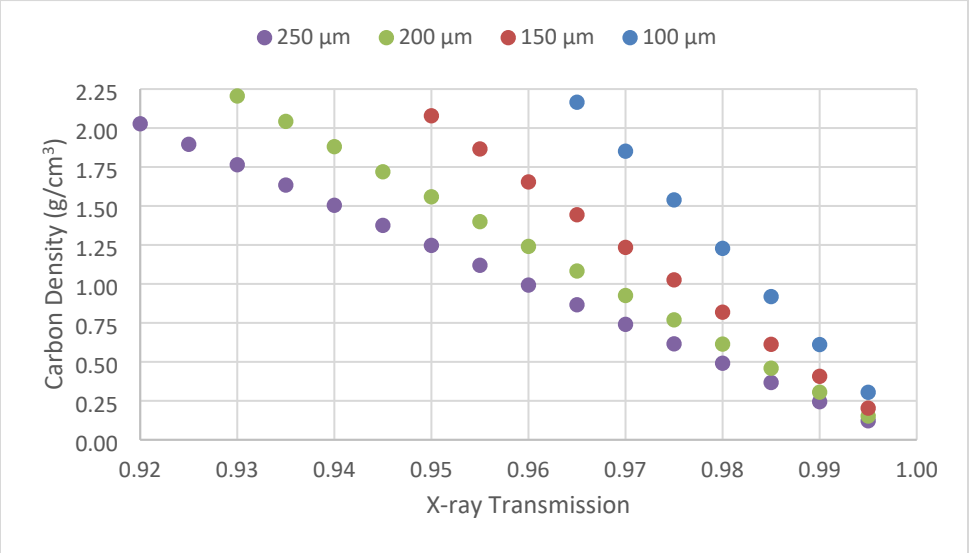

Figure 10. Dependence of calculated carbon density on measured x-ray transmission for various sample thicknesses.

Given the potential for stochastic variation in x-ray transmission to strongly affect the calculated buffer densities, repeated tests were performed on one particle from each sample set. In these tests a single particle was imaged five times in the exact same position with a reference image at a set area on the Kapton tape being acquired between each sample image. Results are shown in Table 3. For particle P2 in the thicker ZrX05-33T sample the mean x-ray transmission was 0.9400 with a standard deviation of 0.0035, while for particle P1 in the thinner ZrX05-31T sample the mean x-ray transmission was 0.9724 with a standard deviation of 0.0059. The thinner sample in this case had a higher standard deviation and based on the calculations shown in Figure 10 would also has a greater shift in calculated density for any variation in x-ray transmission. The range of calculated densities for ZrX05-31T spanned by one standard deviation in x-ray transmission is 1.668–2.585 g/cm^3, while the range of calculated densities for the thicker ZrX05-33T particle using the same criteria is 1.975–2.228 g/cm^3. Both of these ranges are significantly higher than the nominal density of TRISO buffer, likely due to infiltration of the buffer by Crystalbond during sample preparation as has been previously discussed. However, the range of variation is worth consideration. For the method to be of use as QC measurement of TRISO buffer density within a typical specification, the stochastic variation in x-ray transmission will need to be further reduced. This will likely entail thicker samples (within the confines of Figure 1), removal of the Kapton tape to minimize x-ray filtering, and potentially shifting to a more stable x-ray system.

Interestingly, although the range of densities represented by plus-or-minus one standard deviation in x-ray transmission were high relative to the needs of a QC method, they were lower than the range of variation observed between particles of the same material in Table 2. This indicates another source of stochastic error and is a further indication of variable levels of Crystalbond infiltration within the different buffer samples.

Table 3. Repeatability results for x-ray transmission in two particles.

Sample	Transmission						
	Image 1	Image 2	Image 3	Image 4	Image 5	Mean	Std. Dev.
ZrX05-33T P2	0.9350	0.9414	0.9428	0.9430	0.9376	0.9400	0.0035
ZrX05-31T P1	0.9622	0.9742	0.9733	0.9765	0.9760	0.9724	0.0059

6. OPPORTUNITIES TO IMPROVE THE EXISTING APPROACH

Several challenges were identified with the initial approach used for radiography measurement of buffer density in TRISO particles. Unfortunately, due to the limited scope of this initial evaluation of potential methods, these challenges were not resolved. However, they present clear opportunities for future work.

First, although the Kapton tape used to encapsulate the calibration materials and samples was accounted for in image referencing, the relatively low attenuation of x-rays by the thin sections of buffer being analyzed makes removal of any potential sources of uncertainty critical. An alternate method of producing spherical sections of TRISO particles by mounting an array of particles in epoxy, cutting away excess epoxy, then grinding from both sides of the resulting puck should remove the need for Kapton or other encapsulating materials and maximize the number of low-energy x-rays reaching the sample to potentially interact with the buffer layer. This method would also remove the need for Crystalbond epoxy for mounting particles, which may have remained within pores of the buffer layer and significantly affected x-ray attenuation. Finally, this approach would generate a large statistical sampling of spherical segments of TRISO particles in a single step and would thus be more appropriate as a full-scale quality control method.

Second, the quality of the calibration for x-ray attenuation in carbon may be improved by procuring reference materials of known density which span the range of sample thicknesses of interest for spherical sections of TRISO particles. While the calibration curve in Figure 3 shows a good fit overall, the quality of the fit is lowest at the low end of the calibration curve, which is the region most representative of the samples measured. In addition, if this method is to be extended to the other TRISO layers, then appropriate calibration standards for SiC should be acquired as well. Greater rigor can also be applied to the determination of density for the calibration standards to minimize uncertainty in the calibration.

Third, while the Versa 620 used in this work provides a range of x-ray energies and multiple detectors spanning a wide range of magnifications, the source power is relatively limited when operating at low voltage as is desirable when measuring attenuation in low-Z materials. In addition, as was noted in Section 4, the x-ray source in this microscope has stability issues at low power. Greater stability and greater power while operating at low voltage could be achieved by shifting to a different system. For example, the MicroXCT-400 system at ORNL has a source capable of operating at 8W while at 40kV, nearly thrice the power of the Versa 620 source at the same voltage and more stable over time once properly warmed up. The greater power would increase the total counts per unit time spent imaging. Overall, it is expected that the MicroXCT-400 system will reduce stochastic error in x-ray transmission.

7. CONCLUSIONS AND RECOMMENDATIONS

Several potential approaches for measurement of the density of the buffer layer in TRISO particles have been considered in this work. The most promising approach based on radiography of spherical sections from TRISO particles has been tested on surrogate particles with the calibration of x-ray attenuation in carbon based on radiographs of Grafoil. The initial results for buffer density based on this method were variable and consistently higher than densities reported by established methods in interrupted coating runs, indicating several challenges which must be addressed if this approach is to be implemented with accuracy and consistency.

First, a new method for producing and mounting spherical particle sections should be developed which removes uncertainties introduced by encapsulating Kapton tape and residual Crystalbond which may infiltrate the buffer layer. Mounting particles in epoxy, cutting away excess, then grinding both sides to produce a disk with a large number of embedded spherical sections is thought to be a promising approach which would also allow for a larger statistical sampling of particles with relatively low sample preparation effort. This would remove a significant source of presumed error in the initial scoping work (infiltration by Crystalbond into the buffer) and reduce the impact of stochastic variation in x-ray transmission by softening the x-ray spectrum interacting with the sample (by removing the encapsulating Kapton, which absorbed some of the low energy x-rays).

Second, better calibration of x-ray attenuation by carbon should be obtained by using traceable calibration standards of known thicknesses and densities which span the region of interest based on the nominal density of buffer and the targeted thickness of the spherical sections. In addition, calibration standards for x-ray attenuation by SiC could also be acquired to extend the method to that layer as well.

Third, the general approach of density measurement by comparison to calibration standards of a known material could be tested on hot-sampled, buffer-only coated particles. This would maximize the thickness of the buffer layer being measured, increasing the total x-ray attenuation and thus reducing the impact of stochastic variation. It would be necessary in this case to know the thickness of the buffer layer as a function of position within the radiograph, which should be reasonably estimated based on the observed particle cross-section in the radiograph. Testing on buffer-only samples would also provide a form of

verification and validation of results from spherical sections to confirm whether sample preparation is affecting results.

Although the initial testing of this method for buffer density measurement encountered challenges which were not resolved in the initial evaluation, there is still potential for a viable characterization method for buffer density based on radiography to be developed. Given the potential of this method to eliminate the mixed RCRA waste stream associated with mercury porosimetry and to expand the current measurement of buffer density by measuring the statistical distribution in density between particles, this method should be pursued further. In addition, there is the possibility that the general method of layer density measurement by radiography could be extended to the other coating layers, eliminating another complex waste stream from liquid gradient density columns. While this initial scoping work was performed on a relatively expensive Versa 620 XCT system already available at ORNL, after this method is successfully developed, it could be performed on a much simpler radiography or lower-resolution XCT system which is more appropriate to an industrial setting. It is probable that this would be the same system as is used for performing low-resolution radiography of particles to check for uranium dispersion indicative of defective IPyC or for rapid XCT scanning of fuel forms to confirm internal geometries (e.g., fuel free zones) and particle counts.

8. REFERENCES

[1] J. Hunn, R. Lowden, J. Miller, B. Jolly, M. Trammell, A. Kercher, F. Montgomery and C. Silva, "Fabrication and characterization of driver-fuel particles, designed-to-fail fuel particles, and fuel compacts for the US AGR-3/4 irradiation test," *Nuclear Engineering and Design,* vol. 271, pp. 123-130, 2014.

[2] C. Griesbach, T. Gerczak, Y. Zhang and R. Thevamaran, "Microstructural heterogeneity of the buffer layer of TRISO nuclear fuel particles," *Journal of Nuclear Materials,* vol. 574, 2023.

[3] S. Kelkar, C. Boushey and M. Okos, "A method to determine the density of foods using x-ray imaging," *Journal of Food Engineering,* vol. 159, pp. 36-41, 2015.

[4] D. Jackson and D. Hawkes, "X-ray attenuation coefficients of elements and mixtures," *Physics Reports,* vol. 70, pp. 169-233, 1981.

[5] "X-ray Mass Attenuation Coefficients," NIST, [Online]. Available: https://www.nist.gov/pml/x-ray-mass-attenuation-coefficients. [Accessed 2024].

[6] D. Phillips and J. Lannutti, "Measuring physical density with x-ray computed tomography," *Nondestructive Testing and Evaluation International,* vol. 30, pp. 339-350, 1997.

[7] B. Heismann, J. Leppert and K. Stierstorfer, "Density and atomic number measurements with spectral x-ray attenuation method," *Journal of Applied Physics,* vol. 94, pp. 2073-2079, 2003.